Polymer 51 (2010) 3436–3444

Contents lists available at ScienceDirect

Polymer

journal homepage: www.elsevier.com/locate/polymer

Processing of nanocomposite foams in supercritical carbon dioxide. Part I: Effect of surfactant

Thi Thanh Van NGO [a,b], Jannick Duchet-Rumeau [a,b,*], Andrew K. Whittaker [c], Jean-François Gerard [a,b]

[a] Université de Lyon, F-69003, Lyon, France
[b] CNRS, UMR5223, Ingénierie des Matériaux Polymères, INSA Lyon, F-69621 Villeurbanne, France
[c] Centre for Magnetic Resonance and Australian Institute for Bioengineering and Nanotechnology, Level 2, Gehrmann Laboratories, Research Road, The University of Queensland, QLD 4072, Australia

ARTICLE INFO

Article history:
Received 12 May 2009
Accepted 19 May 2010
Available online 27 May 2010

Keywords:
Polystyrene
Clay
Foam

ABSTRACT

Polystyrene-clay nanocomposites were prepared by *in situ* polymerization to achieve the better dispersion of lamellar silicates *i.e.* montmorillonite and fluorohectorite and were used to process foams with supercritical CO_2. Clay–Polymer interactions were modulated by varying the surface treatment of clays: a physical interface was formed with the compatible surfactant showing aromatic groups (MMT-benz) and a chemical interface was created after reaction of methacrylate group (MMT-MHAB) with the styrene monomer. The dispersion of nanocomposites and the microstructure of resulting foams are very dependent on the quality of the clay/matrix interface. With the compatible clay, exfoliation of aromatic clay in polystyrene matrix is obtained at all scales. On the other hand, with the reactive clay, intercalated primary particles are obtained but the size of foam cells is the smallest and cell density is the highest. Our results suggest that the nucleation occurs primarily on physico-chemical nucleation sites that are the carbonyl group of the tethered copolymers synthesized on reactive clay and that present a strong affinity for CO_2. The relaxation times determined by using solid-state NMR spectroscopy are consistent with the formation of the *in situ* copolymers.

1. Introduction

Thermoplastic foams have diverse applications in everyday life. Insulation, packaging and structural applications are some of the major applications of olefinic and styrenic foam products. The addition of nanoclay to the foamed thermoplastic may benefit both foam microstructure [1] and mechanical properties [2]. On the one hand, clay particles may serve as nucleation agents for bubble generation and on the other, the perpendicular alignment of clay particles to the polymer chain stretching direction improves the strain-induced hardening which is required to withstand the stretching force applied during the bubble growth. However dispersion of the nanofillers remains a critical parameter to be tailored either by processing or by chemistry of the polymer/clay interface. To disperse nanoclays in an appropriate polymer matrix, three main methods can be used including melt mixing, solution casting and *in situ* polymerization. Although all of these methods have been somewhat effective in producing nanocomposites, melt mixing and solution casting primarily result in intercalated nanocomposites whereas *in situ* polymerization provides a range of dispersion from intercalated to exfoliated. Whatever the process used, it is essential that there is compatibility between polymer and clay to obtain well dispersed nanocomposite materials. However, the hydrophilic nature of clay prevents its homogeneous dispersion in the organic matrix. To overcome this difficulty, two classical ways can be used either generating polar groups on the matrix chains such as for example, polar oxazoline groups in a styrene copolymer to ensure the compatibilization between montmorillonite and polystyrene [3], or making organophilic the clay surface before its introduction in the polymer matrix. In this last case, the modification takes place mainly in the clay galleries through cationic exchange [4] and extends on the outer surface after grafting of organosilanes on the edges of clay sheets [5].

New techniques, capable improving the properties of polymeric materials and the environmental compatibility of their manufacturing processes have received recently large attention by researchers in the field of material science. Foaming using supercritical carbon dioxide technology is one of these techniques. The CO_2 supercritical fluid presents many advantages for the foaming process [6–8]. Firstly, the use of supercritical CO_2 as foaming agent can offer significant

* Corresponding author at: CNRS, UMR5223, Ingénierie des Matériaux Polymères, INSA Lyon, F-69621 Villeurbanne, France. Tel.: +33 4 72438548; fax: +33 4 72438527.
E-mail addresses: jannick.duchet@insa-lyon.fr (J. Duchet-Rumeau), a.whittaker@uq.edu.au (A.K. Whittaker).

0032-3861/$ – see front matter © 2010 Elsevier Ltd. All rights reserved.
doi:10.1016/j.polymer.2010.05.039

environmental advantages. Secondly, porous materials produced using supercritical carbon dioxide technology also are very much attractive in biomedical applications because the supercritical CO_2 fluid is a non-toxic substance, fast and easy drying. Thirdly, the "pore collapse" phenomena can be avoided by using supercritical CO_2 because it does not give rise to a liquid–vapor interface since at the critical point, the density of the gas phase becomes equal to that of the liquid phase. Moreover, the modification of the nanopores is often difficult because organic solvents are often too viscous to fill such small pores. This effect does not occur with supercritical CO_2 technology because supercritical CO_2 has a viscosity lower than organic solvents and can not condense in the liquid state. From an industrial point of view, CO_2 is inexpensive, non-toxic, non-flammable and easily available with a high degree of purity. Considering all of these advantages, CO_2 seems an excellent foaming agent.

The foaming process includes two thermodynamic stages: a) saturation of polymer by CO_2 fluid and b) cell nucleation and growth. These stages are applied not only to discontinuous but also to continuous processes. The homogeneous theory of cell nucleation is often used to explain the mechanism of formation of the foams. After polymer swelling in supercritical fluid CO_2, a phase separation is necessary to then form pores in the polymeric matrix. During the CO_2 release stage, the pores continue to be formed in the areas rich in polymer and the cells grow according to two mechanisms: by the diffusion of CO_2 in the areas rich in polymer and by CO_2 evaporation. The cell growth by CO_2 evaporation can only occur if the polymer is plasticized and is in the rubbery state.

In the case of a ternary system such as supercritical CO_2/polymer/nanoclay, there is no longer a homogeneous liquid state between the three phases, therefore the heterogeneous theory of nucleation is adopted [9,10]. Heterogeneous nucleation occurs when a third phase is formed with the interface of two other phases, like a gas bubble at the interface of a liquid and a solid [11]. Recently, Siripurapu *et al.* [12] have explained the mechanism of nucleation by using a mixture of homogeneous and heterogeneous nucleation modes. According to Colton [13], the presence of heterogeneous nucleation sites does not preclude homogeneous nucleation. Even when heterogeneous nucleation is energetically favored to occur, homogeneous nucleation can still occur simultaneously with heterogeneous nucleation if the activation energy barrier for homogeneous nucleation can be overcome. Although the mechanism of nucleation is not always well understood, it is generally known that the size, the shape and the distribution of the particles, as well as the surface treatment can affect the effectiveness of nucleation [14].

In this paper, our objective is to study the effects of surfactant chemistry on both the tailoring of nanoclay dispersion within a polystyrene matrix and on resulting foam microstructure. The polystyrene/lamellar silicate nanocomposites are formed by *in situ* polymerization to ensure the best dispersion. The effect of nanocomposite processing will be dealt with in a further paper. Two surface modifications of montmorillonite by cationic exchange have been investigated. Both surfactants are based on a quaternary ammonium cation bearing either a benzyl group to ensure high compatibility with the polystyrene matrix or a vinylic bond to make the surfactant reactive towards styrene monomer. Two kinds of polystyrene/montmorillonite interfaces will be generated in order to study the key role of chain mobility at the interface on foaming.

2. Experimental

2.1. Organophilic layered silicates preparation by cationic exchange

2.1.1. Pristine layered silicates

The non-modified layered silicates that we have selected for these studies belong to the family of 2:1 phyllosilicates. The first of these is a fluorinated synthetic mica, known as fluorohectorite, synthesized by heating talc in the presence of Na_2SiF_6 for several hours in an oven at high temperature. Mica, whose trade name is Somasif ME100, was supplied by Co-op Chemical Co. (Japan) and its exchange capacity (CEC) is around 80 meq/100 g. A partial exchange of Al^{3+} ions in the octaedral layer with divalent ions, for example, Mg^{2+}, leads to negatively charged layers. These negative charges will be replaced by monovalent cations, for example, Li^+ or Na^+, which are exchangeable [15].

The second layered silicate is a natural montmorillonite provided by Süd Chemie (Germany) and is called Optigel EXO255. It has been enriched by Na^+ ions, which are often chosen as compensating ions because they are more sensitive to hydration and promote expansion of the montmorillonite in water. The characteristic parameters of these both pristine lamellar silicates are given in Table 1.

2.1.2. Modified layered silicates

The first modification was achieved with 2-methacryloyloxyethyl hexadecyldimethyl ammonium bromide surfactant (denoted as MHAB), which s the silicate surface not only organophilic but also reactive thanks to methacrylate group by which copolymerization with vinyl monomers may be possible. This reactive cationic surfactant 2-methacryloyloxyethyl hexadecyldimethyl ammonium bromide (MHAB) was synthesized in house by a quaternarization reaction as shown in Scheme 1 and as described in reference [16].

The successful result was checked by ^{13}C NMR spectroscopy that clearly witnesses to the vinylic bond. The NMR results are similar to those reported in the literature [17,18].

Sodium montmorillonite and sodium fluorohectorite were made organophilic by a cation exchange reaction. The clays (6.25 g) were dispersed in 400 ml of deionized water under mechanical stirring at room temperature. The quantity of MHAB (0.1 M) necessary to ensure the surfactant/clay stoechiometry equal to 2 CEC was slowly poured into the clay suspension. The suspension was stirred for 24 h at room temperature. The exchanged clay was then filtered using a Bush filter and washed in two steps: six times with deionized water and six times with the water-ethyl alcohol (50:50) mixture so that no bromide ions were detected by addition to a 0.1 N $AgNO_3$ solution. The modified clays are denoted mica-MHAB and MMT-MHAB.

The second modification uses benzyldimethyl tallow alkyl ammonium ions, bearing an aromatic group that should promote interactions with the chains of the polystyrene matrix. This surfactant will act as a compatibilizer between the silicate fillers and the matrix. In our paper, this modified clay is denoted MMT-benz.

Both surfactants are schematically drawn in Fig. 1.

Table 1
Parameters of pristine lamellar silicates.

	Mica or Fluorohectorite	Montmorillonite
Notation	mica	MMT
Trade name	SOMASIF ME100	OPTIGEL EXO255
Supplier	Co-op Chemical Co. (Japan)	Süd Chemie (Germany)
Nature	Synthetic	Natural and sodium activated
Mineral Formula	$Na_{2x}Mg_{3-x}Si_4O_{10}(F_yOH_{1-y})_2$ $x = 0.15–0.5$ $y = 0.8–1.0$	$Na_x(Al_{4-x}Mg_x)$ $Si_8O_{20}(OH)_4$ $x = 0.5–1.3$
Basal spacing-d_{001} (Å)	12.2	12.3
Cationic exchange capacity (meq/100 g)	70–80	91
Aspect ratio	from 500 to 4000	from 100 to 1000

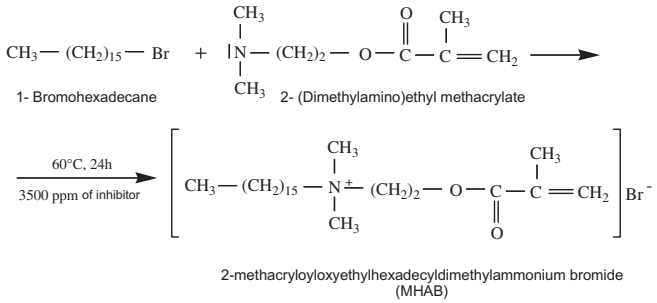

Scheme 1. Quaternarization reaction for synthesis of MHAB reactive cationic surfactant.

2.2. Nanocomposite preparation by in situ method

All the chemicals, styrene monomer, potassium persulfate initiator, sodium dodecyl sulphate (SDS) initiator were purchased from Aldrich and were used as received.

The polymerization of modified layered silicates with styrene was achieved by emulsion in distilled water including several stages. The silicates previously mixed with styrene were allowed to swell at low temperature (4 °C) for at least 24 h. A stirring with sonication was applied to the clay-styrene suspension at room temperature for 2 h before polymerization. In order to reduce the polydispersity index, the SDS surfactant was added in two steps. During micelle formation, the amount of surfactant must be higher than the critical micellar concentration but not in excess f the monomer amount in order to tailor the polymerization. The remaining surfactant was added before the end of polymerization [19]. The polymerization was carried out at 80 °C for 2 h under mechanical stirring (at 100 rpm). The reactive mixture was made of 5.5 g of modified silicate, 1 mol of styrene, 0.04 mol of sodium dodecyl sulfate like surfactant, 0.005 mol of potassium persulfate as initiator mixed within 1 L of distilled water. Then, the particles were precipitated with methyl alcohol to recover the PS/modified silicate (5% wt.) nanocomposite. Purification was carried out by washing this mixture 6 times with distilled water and then 6 times with a water/ethyl alcohol (50 vol. %) mixture. For this step, the reaction yield was 91.5 wt.%. The PS-clay nanocomposite was dried in an oven under vacuum for 24 h. A molecular weight of 400,000 with a polydispersity index of 3 was obtained for neat PS. The nanocomposites have similar molecular weight demonstrating that the presence of clay does not modify the macromolecular chain structure. The glass transition temperature was the same for unfilled and filled polystyrene at about 105 °C.

2.3. Foaming process in autoclave

The batch foaming assembly consists of a pressure cell with a capacity of 300 ml made by PARR Instruments (series 4560). A uniform temperature distribution in the cell is achieved by placing the entire cell in an oven with a control in series of heating and cooling elements. Gaseous CO_2 was fed to the cell. While a pressure transducer continually monitors the cell pressure, a computer-interfaced control valve regulates the overall system pressure. The maximum temperature and maximum pressure can reach 350 °C and 200 bar, respectively. For each experiment, a disk with a 30 mm diameter and 1.3 mm thickness was cut from nanocomposite samples and placed inside the reactor chamber. The foaming process follows four stages:

i) saturation of the sample with supercritical CO_2 for 6 h, at 90 °C, under 10.7 MPa
ii) cell nucleation when CO2 pressure decreases (depressurization rate is 105 Pa. s^{-1})
iii) cell growth up to an equilibrium size during the release of CO_2
iv) vitrification of foam cells when the temperature is reduced below the polymer T_g

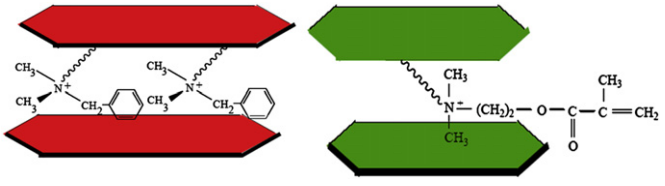

Fig. 1. Schematic representation of the both surface treatment performed on lamellar silicates.

2.4. Material characterization

2.4.1. Wide angle X-ray diffraction (WAXD)

X-ray diffraction (XRD) is widely used to quantify the interlayer spacing of crystalline structures. If the choice of the surfactant is judicious, the nanoclay d-spacing is increased. XRD patterns of the samples were obtained using a Siemens D500 Diffractometer with back monochromator and Cu anticathode (step 0.02, step time 2 s). Special attention was paid to the low 2θ region for accurate determination of d_{001}, *i.e.* the nanoclay *d*-spacing.

2.4.2. Thermo-gravimetric analysis (TGA)

The thermal stability of modified fillers was studied by thermogravimetric analysis using a TGA2950 from Thermal Analysis Instruments using a heating rate of 20 °C/min speed. The weight loss due to the formation of volatile products after degradation at high temperature was monitored as a function of temperature.

2.4.3. Nuclear magnetic resonance analysis (NMR)

Liquid NMR analysis was used for identifying not only the MHAB structure but also the (MHAB-co-PS) grafted nanoclay structure. As NMR in solution is not able to distinguish between a mixture of "nanoclay-MHAB + PS" from the (MHAB-PS) grafted nanoclay, this latter must be washed thoroughly (with the soxhlet) to remove the molecules of MHAB and PS which grafted onto the nanoclay. The ^{13}C NMR experiments are carried out on a Bruker DRX 400 spectrometer operating at 100.63 MHz. Analyses were carried out either at room temperature or 50 °C. For each sample, 60 mg of the (MHAB − PS) grafted nanoclay was solubilized in approximately 0.5 ml of $CDCl_3$ with the addition of several drops of DMSO to improve solubilization.

All solid-state NMR experiments are performed at the University of Queensland on a Bruker AMX300 spectrometer, using a standard Bruker 4 mm cross-polarization magic-angle spinning (CPMAS) probe. In all experiments the ^1H and ^{13}C pulse times are 5 μs, corresponding to a B_1 field of 50 kHz. ^{13}C CPMAS NMR spectra are measured using the standard pulse sequence with a cross-polarization contact time of 1 ms. Partially ^1H $T_{1\rho}$ relaxed ^{13}C NMR spectra are measured after initial spin locking of the ^1H magnetization for the time specified in the text. Values of ^1H $T_{1\rho}$ relaxation times were determined from the single-exponential decrease in intensity in the ^{13}C NMR spectra for a range of spin locking times. All of the peaks in the ^{13}C NMR spectra decreased at the same rate with increasing spin lock time.

2.4.4. Transmission electronic microscopy (TEM)

The specimens for transmission electron microscopy were prepared by microtoming at room temperature and observed using

a Phillips CM120 transmission electron microscope. The ultramicrotome was used for making the extremely fine sections of a few nanometers by using diamond knife. Indeed, it is important to obtain a thickness lower than 100 nm so that the electron beam can cross the sample. Each sample was observed at different magnifications between 3000 and 160 000 times. For each sample, several cuts were made and observed to ensure the reproducibility of morphologies presented in this paper.

2.4.5. Scanning electron microscopy (SEM)

All the morphological observations of nanocomposite foams were carried out on a Jeol 840A LGS scanning electron microscope with a tension of acceleration of 15 kV. Foamed samples were fractured in liquid nitrogen and coated with gold.

2.4.6. Image analysis

The image analysis was manually performed by using UTHSCSA Image Tool Ver. 1.27 software developed by the Centre for Microbial Ecology, Michigan State University, East Lansing, MI 48824 USA. Many images (on different sample areas) were taken to obtain better statistics. The skin thickness of foams was determined on micrographs from the edge of foams by measuring the perpendicular distance from the outer surface of the sample up to the first bubble detected in that direction. Cell density was calculated from the number of cells/cm^3, Nf, that may be expressed as:

$$Nf = \left(nM^2/A\right)^{3/2}(rc)^{1/2}$$

with n: the number of cells counted on a SEM image (between 100 and 200 cells), M: the magnification, A: the analyzed area (by cm^2), r_c: the ratio between height and width of cell. To estimate the cell size distribution, a polydispersity index was measured by the following ratio:

PDI=dw/dn

With dw : weight average diameter of cells $= \sum d_i^2 n_i / \sum d_i n_i$

dn, number average diameter of cells $= \sum d_i n_i / \sum n_i$

n_i: number of cells and d_i: cell diameter

3. Results and discussion

3.1. Characterization of modified silicates

The organically-modified silicates were characterized by X-ray diffraction and thermogravimetric analysis to check the efficacy of the cation exchange modification, the thermal stability of organic modifier ions and the nature of interactions of the surfactant and silicate.

Intergallery spacings determined by X-ray diffraction on both lamellar silicates before and after modification by modifying ions are reported in Table 2. Both types of treatment (MHAB and aromatic surfactant) lead to a swelling of the clay interlayer spacing. Compared to the basal spacing of sodium montmorillonite or mica, the increase of the basal spacing ($d_{001} \approx 12$ Å) clearly shows intercalation of the cations into the interlayer region. However, a lower d-spacing is obtained when tallow alkyl ammonium ions are used. The presence of the benzene ring leads to tilting of the chains of the alkyl ammonium ion relative to the surface of the sheet because the π electrons of the benzene groups can develop strong interactions with the clay sheets. This leads to a bilayer organization characterized by an interlayer spacing of about 18 Å as described by Lagaly *et al.* [20]. On the other side, the MHAB surfactant induces a higher interlayer distance of approximately 22 Å characteristic of a trilayer organization.

Table 2
Intergallery spacings measured by X-rays diffraction before and after cation exchange.

Clay	MMT	Mica	MMT-benz	MMT-MHAB	Mica-MHAB
d_{001}(Å)	12.3	12.2	19.2	21.5	23.3

Thermogravimetric analysis reported in Fig. 2 completes the knowledge of the modified clay structure. It has been observed that peaks corresponding to weight losses between 150 °C and 250 °C typically indicate the presence of organics which could be simply physisorbed either on the external surfaces of the silicate layers or at their edges. On the other hand, weight losses between 300 and 550 °C correspond to loss of organics intercalated into clay galleries [4]. The work of Yoon et al. [21] confirm that the chains confined between the sheets are relatively stable up to 210 °C because the temperature is not sufficient to break the ionic interactions. Indeed, the ionic bonds of ions intercalated between the sheets break between 250 and 400 °C. Both surface treatments show a similar pattern of thermal decomposition with a first loss of mass starting at around 200 °C attributed to the physisorbed alkyl ammonium ions and the two other weight losses at around 300 °C and 400 °C significant of intercalated chemicals in a same ratio of about 20 wt.%.

All the experimental evidence collected by XRD and TGA show that the cationic exchange with MHAB was successful and the three organophilic lamellar silicates are similar in terms of interlayer spacing and amount of intercalated chemicals between layers.

3.2. Analysis of nanofiller dispersion in the PS matrix

The clay surface treatment aims at improving the wettability of nanofillers by the matrix and let an intimate contact between the

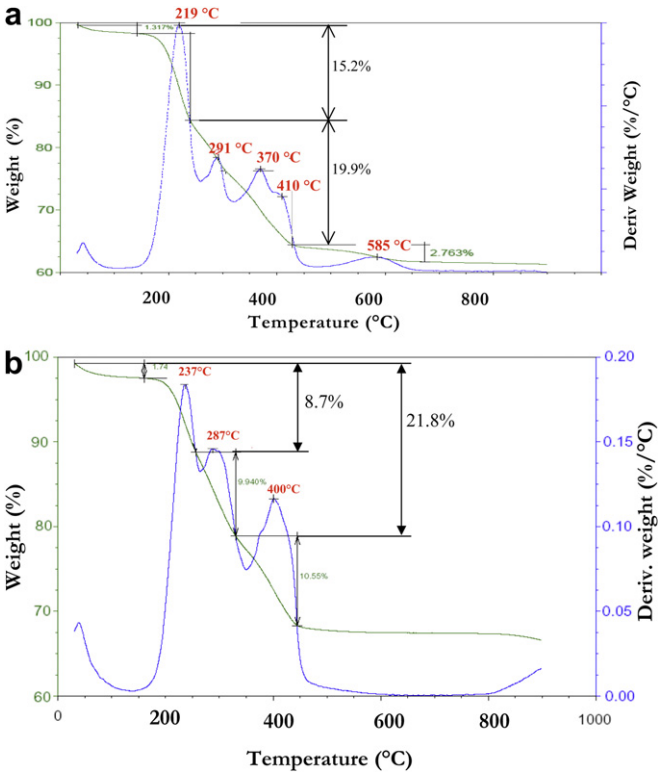

Fig. 2. Thermogravimetric analysis of montmorillonite after exchange with benzyl group (a) and of mica after exchange with MHAB surfactant (b). All the analyzed samples were washed extensively.

nanoclay and the polystyrene matrix. Two different interfaces have been created as a function of the chemical nature of surfactant: *a covalent chemical interface* when the MHAB surfactant is used and *a compatibilized physical interface* when the aromatic surfactant generates Van der Waals interactions towards the matrix. Whatever the chemical structure of the surfactant or the mineral structure of the nanofiller, the polystyrene-nanocomposite synthesized in contact with different modified silicate fillers shows no peak in the WAXD patterns (not shown here). The absence of a peak in the nanocomposite diffraction patterns indicates that a range of morphologies from disordered intercalated to exfoliated could be present and that the polymerization of styrene pushes the platelets apart. Transmission electron microscopy was also utilized to characterize the state of dispersion and the morphology of the clay in the nanocomposites. TEM images collected at low and high magnification are reported in Fig. 3 and characterize the two levels of clay dispersion and distribution in the polymer matrix. The images confirm the results of WAXD analysis by showing a relatively fine nanoscale dispersion, involving layer separation of the clay. The chemical compatibility and physical or chemical interactions between the treated clay surface and intercalated growing species determine the degree of layer separation. Even though these three nanocomposites have a similar nanoscale dispersion as confirmed by WAXD, the mesoscale dispersion and distribution differ and is strongly dependent on the chemical structure of modifying ions and on host structure of clay. Fig. 3a shows a high level of homogeneity with very few areas of intercalated clay particles for nanocomposites processed with MMT-benz. It is well known that the dispersive interactions between the montmorillonite phenyl group and polystyrene can be favourable and lead to formation of a long range clay layer network by the disruption and dispersion of clay tactoïds and aggregates. So, very good dispersion of montmorillonite modified by aromatic alkyl ammonium ion in polystyrene matrix is obtained at all scales. The mesoscale distribution of reactive clays (MMT-MHAB and Mica-MHAB) is insufficient since areas of intercalated primary particles are observed (Fig. 3b) and in a higher amount when mica is used because of its pristine crystalline structure. We tried to explain this difference in final material morphology by investigating the interactions between the modified clay surface and the dispersion medium, *i.e.* styrene monomer.

3.3. Analysis of physical or chemical interactions between modified silicates and styrene monomer

In a first set of experiments, swelling measurements were performed to evaluate interactions at a macroscopic level. The modified clays are introduced progressively to styrene monomer at 4 °C to avoid styrene homopolymerization and left to swell for 144 h, to reach the plateau volume determined for swelling measurements. The swelling ratio can be calculated from volume measurements before (V_{dry}) and after swelling ($V_{swollen}$)using the relationship:

$$S = (V_{swollen} - V_{dry})/V_{dry}$$

The values are reported in Table 3. When fillers evolve from a sol state to a gel state, the swelling ratio varies from 0 to a higher value than 1.

The measured swelling ratios reveal that the lamellar fillers are well dispersed in the styrene monomer under the effect of small molecule diffusion which is evidence of favourable physico-chemical interactions between fillers and monomer. Nevertheless, it would seem that the stronger interactions are obtained with the phenyl group-functionalized montmorillonite. For this latter system, the Π-Π interactions would be stronger and more useful for dispersion than the interactions between methacrylate and

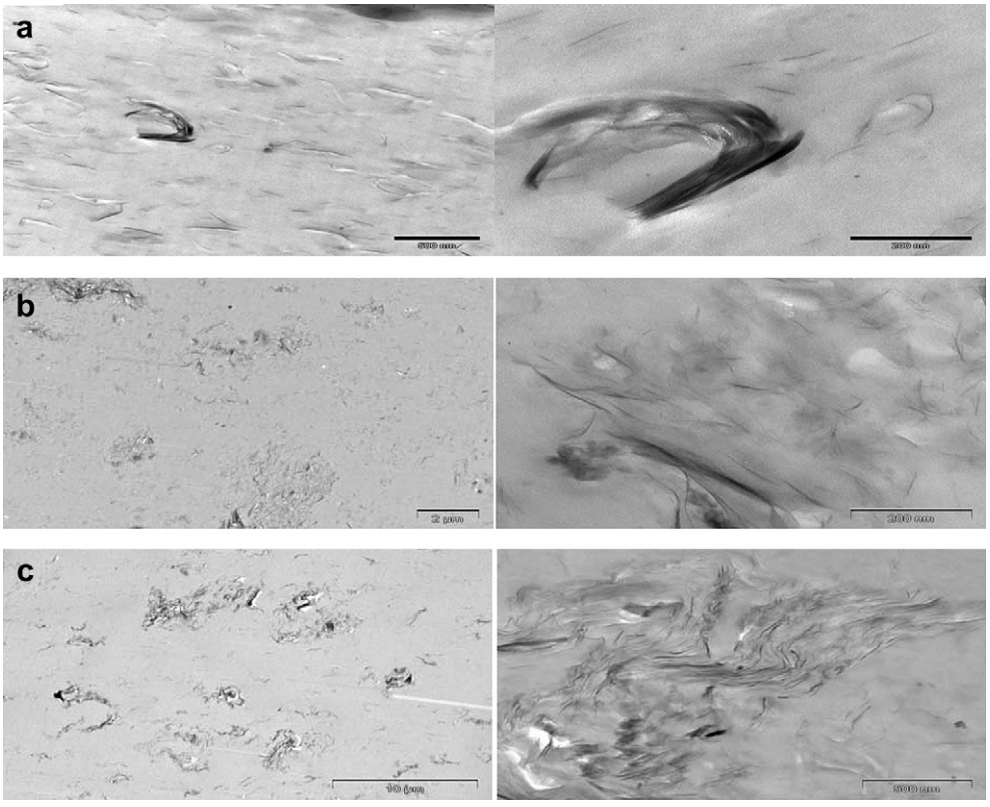

Fig. 3. Transmission electron microscopy images of PS/clay (5% wt.) nanocomposite obtained after emulsion synthesis with MMT-benz (a), MMT-MHAB (b), Mica-MHAB (c).

Table 3
Swelling ratio of different lamellar silicates introduced in styrene monomer at 4 °C.

Modified clay	MMT-Benz	MMT-MHAB	Mica-MHAB
V_{dry} (cm^3)	0.06	0.06	0.06
$V_{swollen}$ (cm^3)	1.5	1.27	1.37
S	**24.0**	**20.1**	**21.9**

styrenic groups. However, reactivity of the double bond carried by the MHAB modifier towards styrene monomer is expected.

Two nanocomposites with different interfaces can be generated as follows:

i) If the MHAB surfactant acts like a vinylic monomer, the styrene monomer inserted into the interlayer gallery may react with the MHAB double bond and synthesize *in situ* a MHAB-PS copolymer. This copolymer grafted covalently onto the silicate surface will be miscible with the polystyrene chains of the matrix and will generate a strong interphase with PS matrix.
ii) If the MHAB surfactant does not react with styrene, only styrene will polymerize and will generate a nanocomposite without strong interactions between lamellar silicates and PS matrix.

To check the nature of the interphase created between MHAB reactive modifier and polystyrene, successive washings were performed to remove all polystyrene chains that have not copolymerized with MHAB. As dichloromethane is known to be a good solvent for polystyrene, an extraction in a soxhlet by using dichloromethane for 24 h is an effective way to isolate the (MHAB-co-PS)-grafted-silicate [16].

The copolymerization between polystyrene and MHAB-modified silicate surface has been examined by ^{13}C nuclear magnetic resonance in solution. As NMR spectroscopy can not distinguish between a simple physical mixing between the silicate-MHAB and PS from MHAB-co-PS grafted silicates with covalent bonds between the organic phase (PS) and the inorganic (silicate-MHAB) phase, it is very essential that the product is exhaustively washed to eliminate all the physisorbed chains on silicate surface and only to analyse grafted copolymers. The ^{13}C nuclear magnetic resonance assignments determined on free MHAB and on (MHAB-co-PS)-mica are listed in Tables 4 and 5 respectively. This NMR analysis shows strong interactions between mica and MHAB-co-PS groups. Indeed, the peaks corresponding to all carbon atoms from C1 to C18 are clearly visible. The carbon C19 and C20 are close to the surface of mica and are immobilized which may highlight strong interactions between mica and modified ions since their signals can not be detected. The peak noted C21 is a quaternary carbon with a chemical displacement δ equal to 135.15 ppm in the pure MHAB, and it is expected at about 44–50 ppm when the MHAB is polymerized. In the mica modified by the possible MHAB-PS copolymer, the characteristic peak would be confused with DMSO and CH and CH_2 groups of polystyrene. The CH_3 denoted C22 of the methacrylate group is no longer visible, giving strong evidence that the double bond has reacted. The corresponding peak of the alpha-methyl carbon would appear from ca. 17–22 ppm, and show splitting due to tacticity and sequence effects. This peak would therefore be difficult to observe after polymerization. In addition, peaks due to double bond carbons (C21 and C23) could not be detected in the ^{13}C NMR spectra of (MHAB-co-PS)-mica, again providing evidence of reaction of the vinyl groups. The ^{1}H NMR results lead to the same conclusions since the loss of vinyl protons is observed (not shown here). Other NMR analyses are in progress in order to further characterize this copolymerization. From the ^{1}H NMR results, the molar ratios of MHAB (0.8%) and styrene (99.2%) can be calculated, based on the integration of benzyl protons (PS) and the end methyl protons of the long alkyl chain. The result agrees well the initial styrene/MHAB molar ratio which is equal to 124: 1.

Table 5
^{13}C nuclear magnetic resonance assignments to (MHAB-co-PS)-mica spectrum.

^{13}C chemical shifts and assignments							
C	1	2 or 15	3	4–14	16 or 18	17	18 or 16
δ (ppm)	14.06	22.63	31.90	29.30/29.60	67.48	51.09	62.71

3.4. Effect of compatible versus reactive interface on the foaming process

A supercritical CO_2 ($scCO_2$) processing method was utilized to prepare nanocomposite foams from PS/clay nanocomposite films processed by *in situ* polymerization. In this case, $scCO_2$ is used as a "reversible plasticizer" that can be easily removed after depressurization. It is this phenomenon of depressed T_g that permits polystyrene to foam at temperatures far below its natural T_g of roughly 100 °C. Incorporation of either a hard (lamellar silicates) or soft (polymer surfactant) additive to PS films is expected to provide internal diffusion barriers, promote nucleation and ultimately, amplify this effect and open new possibilities to obtain polymer foams exhibiting nano/mesoporous morphologies. The purpose of this morphological study is to compare the efficacy of the clay/PS interface, *i.e.* physical (compatible) or chemical (reactive) interface to enhance pore cell density in amorphous polymer films exposed to sc CO_2. PS and PS-5wt.% clay nanocomposites were foamed at 90 °C under a CO_2 pressure of 10.7 MPa. The foam cell morphology is shown in Fig. 4 and Table 6 gathers the results of image analysis carried out on SEM pictures of nanocomposite foams processed with the both kinds of modified nanoclays. After an optimization of foaming processing parameters, PS microcellular foams were successfully created. After foaming, the polystyrene density

Table 4
^{13}C nuclear magnetic resonance assignments to pure MHAB spectrum.

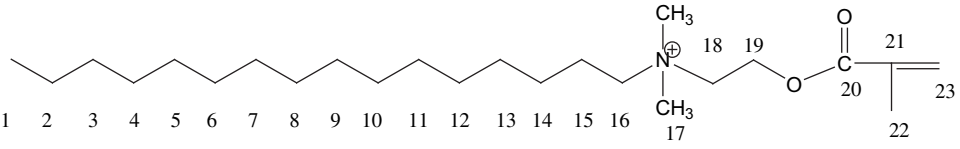

^{13}C chemical shifts and assignments														
C	1	2 or 15	3	4–13	14	15 or 2	16 or 18	17	18 or 16	19	20	21	22	23
δ ppm	14.15	22.97	31.92	29.7029.28	26.28	22.70	65.45	51.88	62.16	58.19	166.37	135.15	18.32	127.46

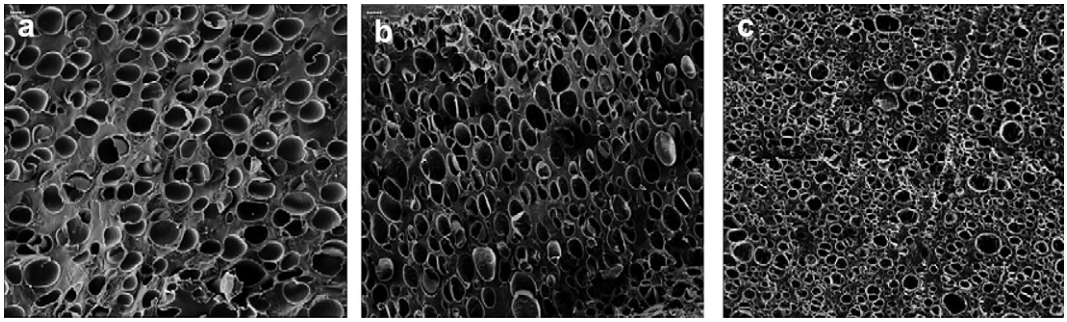

Fig. 4. Morphology of nanocomposite foams by Scanning Electron Microscopy (using magnification ×100): a) PS without clay, b) PS with MMT-benz (5% wt.) and c) PS with MMT-MHAB (5% wt.) (foaming conditions: $T = 90\ ^{\circ}C$, $t = 6$ h, $P = 107$ bar, $v_{released\ pression} = 1.9$ bar/s).

decreased from 1.16 g cm^{-3} to 0.82 g cm^{-3}. The addition of a small amount of clay into the polystyrene matrix decreased by half the density as the density of the foams reached 0.59 g cm^{-3} with the montmorillonite modified with MHAB surfactant. Nanocomposite foams are significantly lighter. The clay may serve as a heterogeneous nucleation agent allowing more sites to nucleate and grow. The thickness of the un-foamed skin decreased in the presence of clay. Indeed, the cell size decreased and the cell density increased. In the presence of 5wt.% MMT-benz, the cell size decreased from 70 μm to 30 μm and the cell density increased from 2.0^{E+05} to 2.4^{E+06} cells cm^{-3}. It is well known that foaming process is strongly dependent on nanofillers dispersion [1]. In the best dispersed nanocomposites, many more individual clay platelets are in direct contact with the polymer matrix and CO_2, providing a much larger interfacial area for CO_2 adsorption and cell nucleation resulting in a higher cell density. While more cells nucleate, a similar amount of gas is available for bubble growth, leading to a reduction of cell size. In others words, the exfoliated nanocomposite foam show the highest cell density and the smallest cell size unlike in intercalated nanocomposites. In this study, the morphology of PS/MMT-MHAB (5% wt.) nanocomposite is less extensively exfoliated than PS/MMT-benz (5% wt.). However, the results do not confirm the expected trends since the cell size was significantly more reduced (18 μm) and the cell density (5.77^{E+06}) was higher for the PS/MMT-MHAB (5% wt.) nanocomposite foam. The chemical nature of surfactant has a significant effect on foaming because the MHAB surfactant functionalized with methacrylate group is CO_2-philic while the benzyl dimethyl tallow alkyl ammonium surfactant presents no group compatible with supercritical CO_2 fluid [22]. The strong affinity between CO_2 and the carbonyl group of the tethered copolymers in PS-MHAB may reduce the gas-particle interfacial tension which leads to a large increase in nucleation rate. Therefore it can be concluded that the exfoliated PS/MMT-benz (5% wt.) nanocomposite has only physical nucleation sites while the exfoliated-intercalated PS/MMT-MHAB (5wt.%) nanocomposite shows physico-chemical nucleation sites. This means that the nucleation occurs primarily on physico-chemical nucleation sites where there are strong interactions with the CO_2 supercritical fluid. The same behaviour was observed with the reactive mica. The details of the foam fabrication are not strongly dependent on the host structure of the lamellar silicate but are strongly linked to the chemical nature of the modifier.

Table 6
SEM image analysis performed on different nanocomposite foams. (foaming conditions: $T = 90\ ^{\circ}C$, $t = 6$ h, $P = 107$ bar, $v_{released\ pression} = 1.9$ bar/s).

Foam sample	Density (g/cm^3)	d_n (μm)	d_w (μm)	PID = d_w/d_n	Cell density ($cells/cm^3$)	Aspect ratio	Skin thickness (μm)
PS	0.8195	73	79	1.09	2.03^{E+05}	1.60	142.3
PS/MMT-MHAB (5% wt.)_	0.5910	18	25	1.39	5.77^{E+06}	1.58	104.3
PS/MMT-benz (5% wt.)_	0.6782	31	38	1.24	2.32^{E+06}	1.74	92.0

3.5. Effect of compatible versus reactive interface on the clay dispersion in the foams

The distribution of lamellar silicates in the foam walls is also dependent on the chemical nature of the surfactant. With the clay compatibilized with the aromatic groups, a “clay fabric” at the cell border is generated as shown by TEM analysis in Fig. 5. In this area, the clay layers are aligned along the interface between polystyrene matrix and CO_2 gaseous phase. The thickness of the “clay fabric” is about 2 μm. Further from the interface, the layer orientation decreases progressively until the clays appear isotropic. This gradual change in morphology is strongly dependent on the CO_2 solubility within the matrix, being preferentially higher at the cell border but also higher with very well dispersed clay particles observed in the initial nanocomposite material which results in sufficient mobility to the clay layers. When the matrix is intimately linked to the silicate surface, with the reactive clay PS-MHAB-MMT or Mica, this gradual structuration is not observed (Fig. 6). The synthesized MHAB-PS copolymers showing a higher viscosity strongly reduce the inorganic layer mobility and prevent orientation of the layer under the effect of supercritical CO_2 fluid during cell growth.

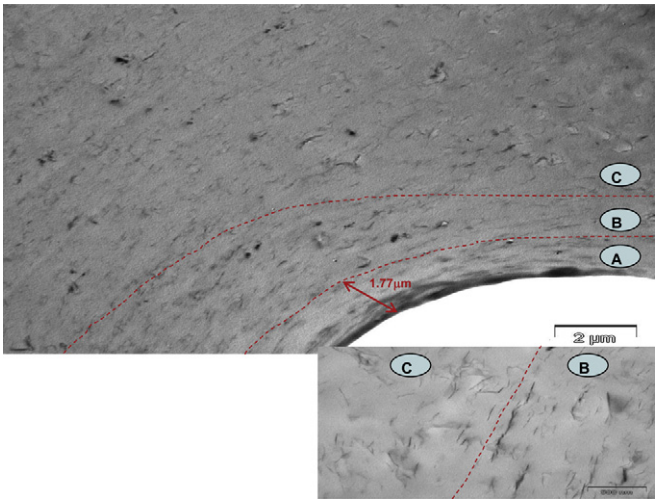

Fig. 5. TEM pictures on layers structuration in the wall of foam cells-PS/MMT-benz (5wt.%).

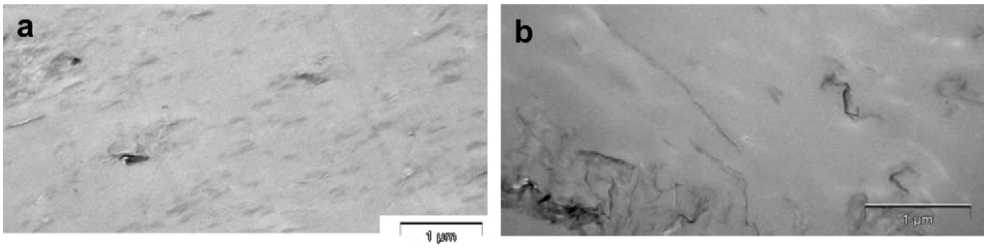

Fig. 6. TEM pictures on the wall of foam cell processed with clays modified with MHAB: a) MMT-MHAB and b) mica-MHAB.

Table 7
^{1}H $T_{1\rho}$ relaxation times measured by ^{1}H nuclear magnetic resonance spectroscopy performed on nanocomposite foams. (foaming conditions: T° = 90 °C, p = 690 bar, t = 6 h, $v_{released\ pression}$ = 1.9 bar/s).

Foam sample[a]	^{1}H $T_{1\rho}$ (ms)
PS/5% MMT-benz with an exfoliated structure	7.1
PS/5% MMT-benz with an intercalated structure[a]	7.5
PS/5% MMT-MHAB obtained by *in situ* polymerization.	7.7

[a] This foam was prepared from melt processed PS/clay nanocomposite.

3.6. Analysis of interactions in nanocomposite foams by NMR technique

To study further the morphology of the nanocomposite foams, we have determined the relaxation times by using solid-state ^{1}H NMR spectroscopy. The longitudinal relaxation times in the rotating frame ($T_{1\rho}$) are reported in Table 7. It is well known that the $T_{1\rho}$ values are at a minimum when the frequency of molecular motions is close to 50 kHz. For glassy polymers, the measured values are an average because of the diffusion of the NMR magnetization due to the strong dipole–dipole coupling between the protons. Previously we have measured under identical conditions a value for the ^{1}H $T_{1\rho}$ for pure PS equal to 8 ms [23].

A single value of ^{1}H $T_{1\rho}$ was measured for the foams prepared with both surfactants. Firstly, this indicates that on a scale of greater than around 10–20 nm the materials are homogeneous [1]. Since spin diffusion averages the magnetization over this length scale, we cannot comment on homogeneity over smaller dimensions. We note also that for all of the foams the measured ^{1}H $T_{1\rho}$ values are slightly less than that previously measured for pure PS. This indicates either that the intrinsic relaxation time of the PS is reduced, for example by plasticization by presence of the particles, and/or that the PS is mixed (better than 20 nm) with other ^{1}H-containing species which have shorter relaxation times; these are likely to be more mobile species, such as methyl groups or alkyl chains. The extent of averaging (reduction) of the relaxation times is greatest for the PS modified with 5wt.% MMT-benz with an exfoliated structure, as expected for a better dispersed system. Comparison with the PS/MMT-MHAB foam is difficult due to possible differences in the intrinsic relaxation times of the MMT-benz and MMT-MHAB nanoclays, however, observation of a single ^{1}H $T_{1\rho}$ relaxation time close the value for pure PS is strong evidence of molecule-scale mixing and suggests the formation of a MMT-MHAB-PS copolymer.

4. Conclusions

Polystyrene/clay nanocomposite were prepared by polymerization of styrene in the presence of lamellar silicates and used to make nanocomposite foams with supercritical CO_2 as the foaming agent. We have shown that the addition of clay can reduce cell size and increase cell density. However, the morphology of these nanocomposite foams are strongly dependent on the surfactant used. Two interfaces were generated: a physical interface when an ammonium surfactant functionalized with aromatic groups is used, and a chemical interface when an ammonium surfactant functionalized with methacrylate group is used which may react with the styrene monomer to form a copolymer. The quality of the interphase between silicate layers and the matrix has a key role both in the dispersion of nanocomposites and in the microstructure of resulting foams. When the clay modified with benzyl groups is used, a highest degree of exfoliation in nanocomposite is obtained due to the compatibility of the surfactant with the polystyrene matrix. On the other hand, when the nanoclay is made reactive towards the matrix, a non-homogeneous morphology is observed because of the MHAB group is less compatible with polystyrene matrix. However, when the reactive clay is used to prepare the foams, the cell size is the smallest and cell density is the highest. The MHAB surfactant behaves as a nucleation agent with CO_2-philic interfaces while MMT-benz acts as a physical nucleation agent that has no specific interaction with the CO_2 supercritical fluid. If the miscibility at the interface polystyrene/clay is a key parameter to enhance the dispersion state, the affinity of the surfactant to CO_2 is essential to ensure a reduction in the nucleation free energy and a large increase in nucleation rate. The relaxation times measured by solid-state NMR spectroscopy confirms homogeneity of the PS phase on the level of greater than 20 nm, and a comparison of the behaviour of the exfoliated with intercalated materials suggests more intimate mixing of the clay layers. The NMR results are consistent with the formation of a copolymer of styrene with the methacrylate-functionalized clays. Work is in progress to have a direct experimental evidence of the copolymerization by using HR-MASS NMR spectroscopy.

Acknowledgments

We thank Pierre Alcouffe and the Centre Technologique des Microstructures for TEM observations, Ruben Vera at the Centre de Diffractométrie Henri Longchambon (Université Claude Bernard Lyon I) for XRD Measurements, Valérie Massardier and Fernande Boisson at the Service Commun de RMN du Réseau des Polymféristes Lyonnais for liquid NMR analysis.

References

[1] Zeng C, Han X, Lee LJ, Tomasko DL, Koelling KW. Adv Mater 2003;15:1743–7.
[2] Nam PH, Maiti P, Okamoto M, Kotaka T, Nakayama T, Takada M, et al. Polym Eng Sci 2002;42:1907–18.
[3] Hasegawa N, Okamoto H, Kawasumi M, Usuki A. J Appl Polym Sci 1999;74:3359–64.
[4] Le Pluart L, Duchet J, Sautereau H, Gérard JF. J Adhes 2002;78:645–62.
[5] He H, Duchet J, Galy J, Gérard JF. J Coll Interf Sci 2005;288(1):171–6.
[6] Reid RC, Prausnitz JM, Poling BE. The properties of gases and liquids. New York: McGraw-Hill; 1987. 741 pp.
[7] Cooper AI. J Mater Chem 2000;10:207–34.
[8] Cooper AI. Adv Mater 2003;15:1049–59.
[9] Strauss W, Ranade A, D'souza NA. 48th Int SAMPE Symp 2003;48(1):1171–80.
[10] Strauss W, Ranade A, D'souza N. AANTEC 2003 2003;61(2):1812–6.
[11] Shaft MA, Flumerfelt RW. Chem Eng Sci 1997;52:627–33.
[12] Colton JS, Suh NP. Polym Eng Sci 1987;27:485–92.
[13] Siripurapu S, Desimone JM, Khan SA, Saad A, Spontak Richard J. Macromolecules 2005;38:2271–80.

[14] Han X, Zheng C, Lee LJ, Koelling KW, Tomasko DL. Polym Eng Sci 2003;43:1261–75.
[15] Reichert P, Kressler J, Thomann R, Muelhaupt R, Stoeppelmann G. Acta Polym 1998;49:116–23.
[16] Zeng C, Lee LJ. Macromolecules 2001;34:4098–103.
[17] Hamid SM, Sherrington DC. Polymer 1987;28:325–31.
[18] Nagai K, Ohishi Y. J Polym Sci Part A 1987;25:1–14.
[19] Bovey FA, Kolthoff IMJ. Polym Sci 1949;5(4):487–94.
[20] Lagaly G. Appl Clay Sci 1999;15:1–9.
[21] Yoon JT, Jo WH, Lee MS. Polymer 2001;42:329–36.
[22] Shen Z, McHugh MA, Xub J. Polymer 2003;44:1491–8.
[23] Thurecht Kristofer J, Hill David JT, Preston Christopher ML, Rintoul Llew, White John W, Whittaker Andrew K. Macromolecules 2004;37(16): 6019–26.